Time-Resolved Optical Tomography in Preclinical Studies: Propagation of Excitation and Fluorescence Photons.

F. Nouizi[1], R. Chabrier[1], M. Torregrossa[2], P. Poulet[*,1]
[1]Laboratoire d'Imagerie et de Neurosciences Cognitives, [2]Laboratoire des Sciences de l'Image, de l'Informatique et de la Télédétection
*Corresponding author: 4 rue Kirschleger, 67085 Strasbourg Cedex, France, patrick.poulet@linc.u-strasbg.fr

Abstract: We present time-resolved methods that rely on near-infrared photons to image the optical properties and distribution of fluorescent probes in small laboratory animals. The scanner assembled in our laboratory is described. The coupled diffusion equations of excitation and fluorescence photons in highly scattering tissues were solved using the three-dimensional Finite Element Method (FEM) provided by Comsol. The computed results allowed to yield photon density maps and the temporal profiles of photons. Simulations were carried-out on two test objects: a resin cylinder and a mouse phantom. The latter required taking into account the straight propagation of photons between the optical fibers and the animal phantom. The results demonstrate the potential applications of the method to pre-clinical imaging.

Keywords: diffuse optical tomography, fluorescence molecular tomography, photon propagation, diffusion equation.

1. Introduction

Diffuse Optical Tomography (DOT) and Fluorescence Molecular Tomography (FMT) are new imaging modalities with promising pre-clinical and medical applications[1]. Both rely on the collection of photons that propagate through scattering media such as tissues, with different source/detector configurations. The emergence of these methods was made possible by the development of new light sources and sensitive detectors, as well as by the construction of new fluorochromes, in the near infrared region, where photons can propagate over distances exceeding several centimeters in living tissues. Excitation photons are detected in DOT, fluorescence photons in FMT. Maps of the optical properties, absorption and reduced scattering coefficients, and of the distribution of fluorochromes can be computed from tomographic measurements[2].

The absorption and reduced scattering coefficients of biological tissues provide essential information about perfusion and blood oxygenation. The development of novel fluorescent probes and reporters opens up new ways to image molecular processes in vivo, such as gene expression, or to monitor therapy[3].

The image reconstruction step in DOT and FMT requires knowledge about the propagation of light in tissues. Two methods are usually used to solve this forward problem[4]:

- the Monte Carlo simulation of the motions of photons encountering scattering and absorption events;
- the resolution of the radiative transfer equation, or photon transport theory, usually simplified to the diffusion equation, where the optical energy diffuses through a concentration gradient.

Our laboratory is involved in the construction of a three-dimensional optical imaging system, dedicated to both DOT and FMT, based on the time-resolved detection of photons. The reconstruction process relies on the diffusion approximation and takes into account the measured temporal information. This paper presents the assembled instrument and the image reconstruction process, with a special emphasis on the resolution of the forward problem using the Finite Element Method (FEM). Some simulated and experimental results illustrate potential applications of these methods in preclinical imaging.

2. Instrumentation

As valuable information can be gathered from the photon propagation time, we built a time-resolved diffuse optical tomography system[5]. The scanner assembled is schematically described and illustrated on Figure 1. Its main components are a multi-channel picosecond laser diode system (Sepia, Picoquant), an 8-anode Micro-Channel Plate Photo-Multiplier Tube

(MCP-PMT, R4110U, Hamamatsu) followed by Time-Correlated Single Photon Counting (TCSPC) modules (SPC 134, Becker & Hickl). The Sepia system can drive up to 8 laser heads operating in synchronous or sequential mode, with a repetition rate up to 80 MHz. Our set-up uses four laser heads, operating at 4 wavelengths (690, 785, 830 and 870 nm), fitted with one quad-furcated 4-to-1 optical fiber (Ocean Optics).

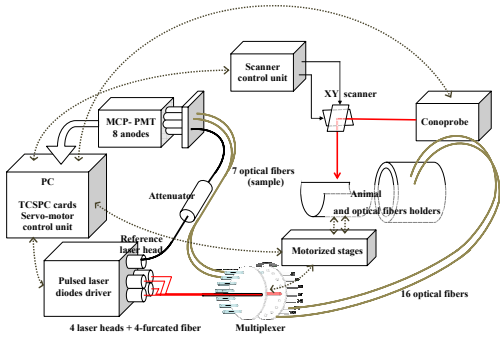

Figure 1. Schema of DOT and FMT system.

The common end of this fiber is mounted on the fixed part of a home-made multiplexer. This device allows to illuminate the object under study with a single optical fiber. This fiber is one out of 16 fibers fixed on the moving part of the multiplexer, all ending on a ring surrounding the area of interest of the object under investigation. At the same time, 7 out of the same 16 fibers, are used to collect light coming out from the object. These 7 fibers are usually placed at angles ranging from 112.5° to 247.5°, by 22.5° steps, from the irradiation fiber. In this configuration, we can analyze the object using a trans-illumination geometry. By rotating the multiplexer by 22.5°, we change at the same time the irradiation and the detection points, while the source/detector mechanical mounting is kept constant.

Seven multimode optical fibers, 1000-µm in core diameter (Ocean Optics), are used to transmit light coming out of the multiplexer to 7 out of 8 light-guides with an end shape adapted to the photocathode of the MCP-PMT. An air-gap between the fibers and the light guides allows the insertion of an optical filter to eliminate excitation wavelengths during fluorescence experiments. The eighth channel is usually used for measuring the time origin and correcting experimental jitter in data.

The electrical pulses delivered by the MCP-PMT are amplified (HFAM, Becker & Hickl) before entering the 8 TCSPC channels.

A no-contact holographic technique using a sensor (Conoprobe, Optimet) and an XY optical scanning system (Cambridge Technology) has been added to the tomography set-up in order to record the coordinates of the surface of the object, or animal as the case may be, under investigation, before it is placed into the DOT/FMT scanner. This information is obviously required for the reconstruction process.

The object, multiplexer and surface imaging device are placed in a home-made black box fixed on a laboratory optical table (63-500 TMC). All the electronic parts and the PC computer which controls the mechanical displacements and acquisitions are placed underneath the table top. Data acquisition is controlled using the software Labview (National Instrument). Data analysis and image reconstruction are performed with customized Matlab applications (Mathworks) and Comsol software.

The main characteristics of the sources and detectors used can be founded in ref 5.

3. Diffuse light transport modeling

Our first experiments were carried out on cylindrical phantoms filling the whole space between optical fibers in the holder. We solved the light transport issue in these samples by considering isotropic light sources at one diffusion length under the point of illumination. A two-dimensional FEM was written with the Matlab software. We computed directly the first moments of the temporal profiles of light coming out of the sample, also called Temporal Point Spread Functions (TPSF), by using the method described by Arridge *et al*[6].

At that stage, the setup was ready for experiments on animals, which require to solve the forward problem in three dimensions, taking into account the emission of fluorescence in the animal. We decided to use Comsol Multiphysics to compute the TPSF corresponding to a given experiment, taking into account the following

parameters: animal shape, source position, 3D optical properties at excitation and fluorescence wavelengths and distribution of the fluorescent probe. The propagation of scattered photons can be described, using the diffusion approximation of the radiation transport equation, as:

$$\frac{\partial u}{\partial t} - \nabla\kappa\nabla u + \mu_a c u = -f(t, r_0) \quad (1)$$

where $f(t,r_0)$ is the distribution of "isotropic" sources; u, the photon density within the object; c, the speed of light; μ_a, the absorption coefficient; μ'_s, the reduced scattering coefficient, and $\kappa = c/3(\mu_a + \mu'_s)$, the diffusion coefficient. The isotropic sources are temporal distributions at a distance $1/\mu'_s$ from the irradiation sites.

The density of fluorescence photons u_2 can be computed from:

$$\frac{\partial u_2}{\partial t} - \nabla\kappa\nabla u_2 + \mu_a c u_2 = -\frac{\eta c}{\tau}(u \otimes e^{-t/\tau}) \quad (2)$$

where η is the quantum yield and τ the lifetime of fluorescence. In this equation, the second term is the convolution product of u (excitation photon density) times the exponential decay of fluorescence. We use the Neumann boundary condition for both u and u_2:

$$\vec{n}\kappa\nabla u + qu = 0 \text{ and } \vec{n}\kappa\nabla u_2 + qu = 0 \quad (3)$$

with q being a function of the reflection at the surface.

4. Methods

4.1 Epoxy resin phantoms

Epoxy resin phantoms were used in order to compare the results of simulations computed with Comsol Multiphysics with those obtained with our former FEM software, but also with experimental data acquired on test objects having the same optical properties. Below, we will present simulation data corresponding to an epoxy resin phantom, obtained with the Comsol 3D object modeling toolbox. The phantom geometry was as follows: cylinder 60 mm high, 40 mm in diameter, centered on x = y = z = 0. The optical background properties were: n = 1.54 (c = 0.2 mm.ps^{-1}, q = 0.023), μ_a = 0.008 mm^{-1}, μ'_s = 0.6 mm^{-1}, κ = 0.108 mm^2/ps at both excitation and fluorescence wavelengths. It contained 3 rods, 8 mm in diameter:

- C1 at position x = 0 mm, y = + 10 mm, 5 times as scattering as the background,
- C2 at position x = - 8.66 mm, y = - 5 mm, twice as absorbing and scattering as the background,
- C3 at position x = + 8.66 mm, y = - 5 mm, 10 times as absorbing as the background and containing a fluorescent dye with η = 0.5, τ = 500 ps. Figure 2 represents the geometry and mesh of the object described.

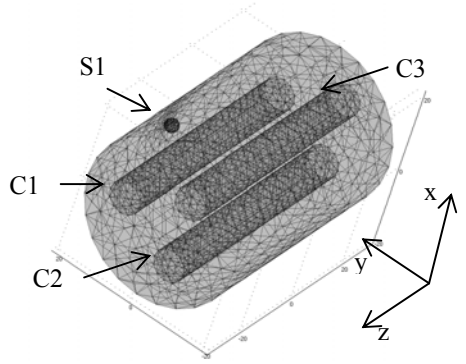

Figure 2. Mesh of the simulated object showing the 3 rods and the isotropic source.

The light beam entered the object at r_0 (x = 0 mm, y = + 20 mm, z = 0 mm), corresponding to an isotropic source S1 of radius 1.67 mm ($1/\mu'_s$) at x = z = 0 mm, y = + 18.33 mm with a temporal profile given by:

$$f(t) = 100 \exp(-0.1t - 200/t) \text{ (t in ps)} \quad (4)$$

4.2 Mouse phantom

In order to test our experimental setup, we made a mouse phantom with a latex envelop molded on a sacrificed mouse and filled with a polyvinyl alcohol/Borax (5/2) gel containing titanium oxide and black India ink. The expected optical properties of this phantom were μ'_s = 0.6 mm^{-1} and μ_a = 0.008 mm^{-1} to model biologic tissues. A micro-tube, 10 times as absorbing, and containing 5 µM Indocyanine green (ICG) was inserted in the head of the phantom, to produce a fluorescent volume simulating a pathology to be detected in the animal phantom.

To produce the virtual model of this phantom with Comsol, the surface of the back and sides of

the mouse phantom was scanned with the holographic system. The entire, closed, surface of the phantom was obtained by merging this surface with a previously recorded profile of the 'bottom' surface, corresponding to the cylindrical bed of the animal holder of the tomography setup described above. The 3D solid object finally obtained is shown on Figure 3. A cylinder was then added to simulate the fluorescent tube inserted in the physical mouse phantom. The resulting 3D object was subsequently used as an analyzed geometry for the Comsol FEM structure.

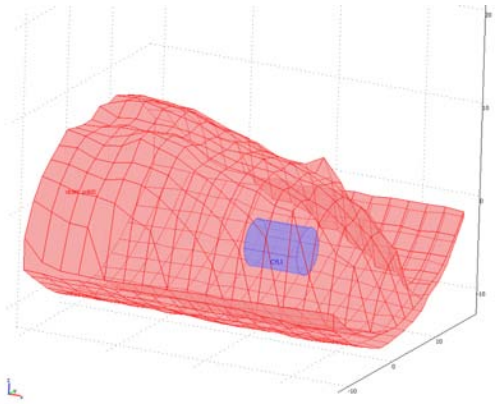

Figure 3. The 3D solid object used for the simulation of diffuse light propagation in a mouse phantom.

The use of equation (1) requires knowledge about the distribution of isotropic light sources, at a distance $1/\mu'_s$ from the incident point of the illuminating beam, originating from one optical fiber and reaching the surface of the animal phantom. The temporal profiles of the photon density in the phantom body and of photon fluxes leaving it at any node of the surface can be computed by solving equation (1) for DOT experiments or the system of equations (1) and (2) for FMT experiments. Light entering the output fibers can then be computed from knowledge about the phantom surface, and the position and characteristics (size, orientation and numerical aperture) of the fibers.

4.3 Computing isotropic light sources.

This subsection describes how we computed the distribution of light sources in the animal phantom, generated by the picosecond laser beam at the exit of a given optical fiber. Light pulses simulated with equation (4) had a width equal to 35 ps.

The distribution of light in the air gap between the fiber and the surface of the phantom and the fiber was modeled as a cone having its apex at the excitation fiber, its base lying in the plane containing the center of the detection ring of the tomography set-up, and an angle at the apex as a function of the numerical aperture of the optical fiber. The isotropic source, at $1/\mu'_s$ below the surface consisted of the nodes closest, from that distance, to the surface within the illumination cone as shown on Figure 4.

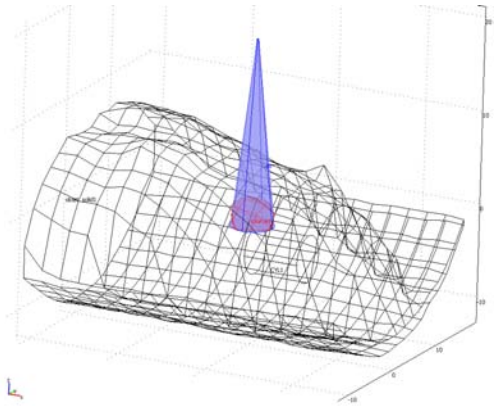

Figure 4. Illumination of the animal phantom by an excitation fiber and position of the isotropic source.

The subsequent steps consisted in meshing the analyzed geometry, as shown on Figure 5, setting the parameters in all sub-domains and solving the diffusion equations. All nodes of a given sub-domain had the same parameters in these simulations, which can be considered as the first step of the reconstruction problem.

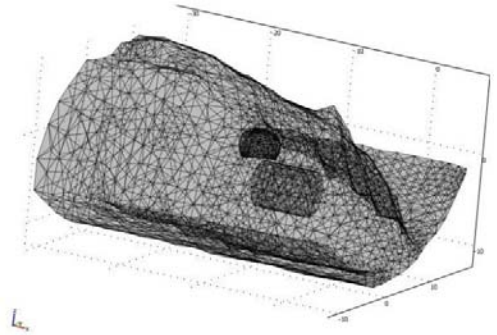

Figure 5. 3D mesh of the analyzed geometry

4.4 Computing temporal profiles.

The final step was the computation of the temporal profiles of light entering a given optical fiber. These TPSF could then be compared to experimental results. We modeled light admission in the fiber in the same way as we did the illuminated area on the surface of the animal phantom. Knowing the photon density in each node n_i of the mesh allowed to determine which mesh elements on the surface belonged to the fiber light admission cone. Each element was characterized by its normal vector $\vec{n}$ and by the photon density Φ at its center of gravity "g":

$$\Phi(g,t) = \frac{d_1}{D}\Phi(n_1,t) + \frac{d_2}{D}\Phi(n_2,t) + \frac{d_3}{D}\Phi(n_3,t) \quad (5)$$

where Φ is the photon density at time t, n_i are the 3 nodes of the element, d_i is the distance between the center of gravity and the node n_i and $D = d_1 + d_2 + d_3$.

The surface of the object was assumed to exhibit a Lambertian reflectance: i.e. a density of photons decreasing as a function of the cosine of the angle α between the normal vector $\vec{n}$ and a vector pointing from the center of gravity of the mesh element to the fiber. The TPSF measured for each fiber was then proportional to:

$$\Phi(f_j,t) = \left(\sum_{1}^{N_j} \Phi(g_i,t) A_i \cos(\alpha_i) L / R_i \right) / \left(\sum_{1}^{N_j} A_i \right) \quad (6)$$

The i^{th} element illuminating fiber "f_j" had a photon density $\Phi(g_i,t)$, an area A_i , an angle α_i. It was at a distance R_i from the fiber, the diameter of which was L. The sum was carried out on the N_j elements encompassed in the illumination cone of fiber f_j.

5. Results

Time-resolved 3D photon density maps and TPSF were obtained with the methodology reported above.

5.1 Epoxy resin phantoms

As an example, the 2D photon density maps, measured 2 ns after the excitation pulse, in the plane z = 0, are shown on Figure 6. Excitation photons are shown on Figure 6.a, fluorescence photons on Figure 6.b.

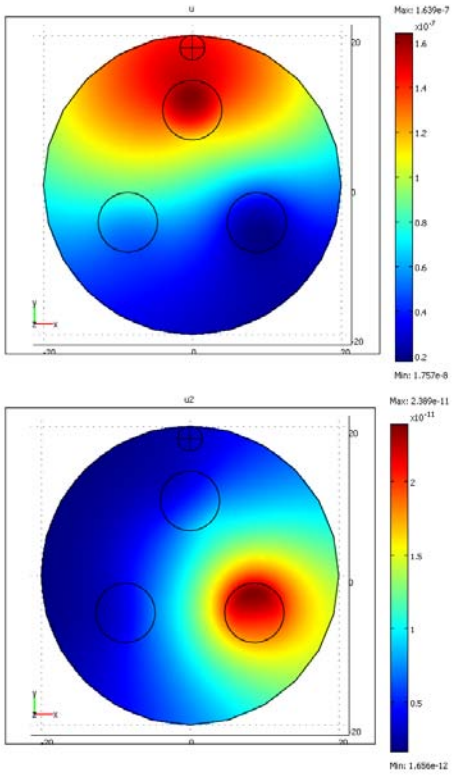

Figure 6. Excitation (top) and fluorescence photon (bottom) density maps, 2 ns after the light pulse in the z = 0 plane. Phantom described in subsection 4.1.

The temporal profiles of photons coming out of the object, at excitation and fluorescence wavelengths, were then computed from the density maps for the nodes of interest on the outer surface.

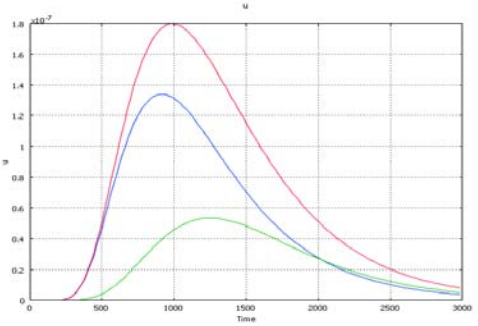

Figure 7. TPSF of excitation photons detected at 180° (green), - 120° (blue) and + 120° (red) from the illumination fiber.

TPSF at three different positions are shown on Figure 7 (excitation wavelength) and on

Figure 8 (fluorescence photons). The positions, given by the angles between the illumination fiber and the detection fibers were: 180° (green), - 120° (blue) and + 120° (red). The blue curve corresponds to the fiber facing the most absorbing and fluorescent rod C3, the red one to the fiber facing the more absorbing and scattering rod C2. We can observe from Figure 7 that a more absorbing area reduced the TPSF and that a more scattering area enlarged it.

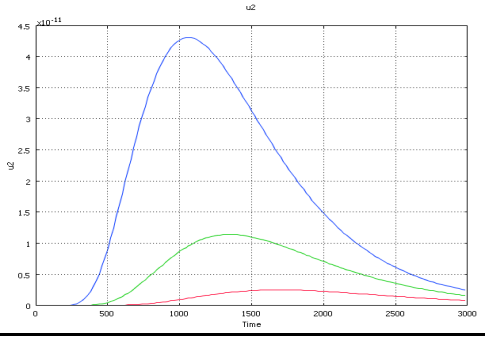

Figure 8. TPSF of fluorescence photons detected at 180° (green), - 120° (blue) and + 120° (red) from the illumination fiber.

The intensity and mean time of the TPSF measured at the fluorescence wavelength strongly depends on the position of the fluorochromes in the phantom, as shown on Figure 8.

5.2 Mouse phantom

In this section, we will present 3D photon density maps of the surface of the animal phantom. The viewing point was set in front of the phantom, slightly under the holder's plane. This vantage allowed to see the head of the animal phantom and the lower part of the holder and so compare two kinds of experiments that can be made with our setup, using reflection and trans-illumination geometries. The TPSF computed for 3 optical fibers in the vertical plane of the illumination light beam will also be discussed. Excitation and fluorescence photons will both be considered.

The photon density maps at the surface of the animal phantom were measured 500 ps after the excitation pulse. Excitation photon maps are shown on Figure 9.a, fluorescence photon maps on Figure 9.b.

The presence of the more absorbing cylinder is clearly shown on Figure 9.a. The fluorescent inclusion is clearly seen on Figure 9.b.

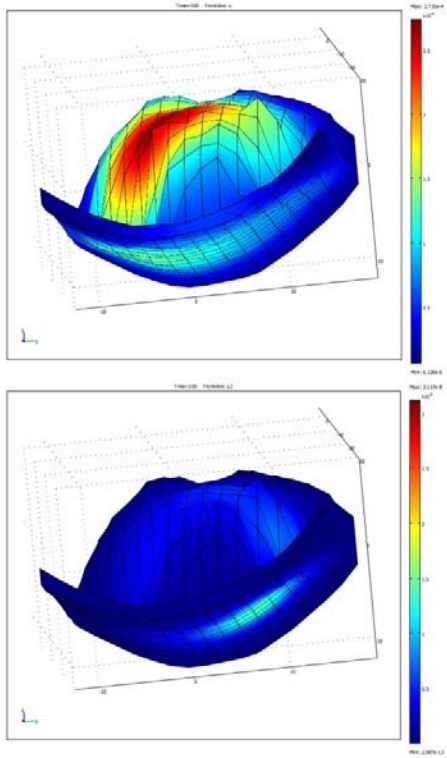

Figure 9. Excitation (top) and fluorescence photon (bottom) density maps at the surface of the animal, 500 ps after the light pulse in a vertical plane. Phantom described in subsection 4.2.

The trans-illumination geometry is more sensitive than reflection geometry in fluorescence experiments. As the former also senses the whole object, it should be more performing for real 3D preclinical imaging.

TPSF at three different positions are shown on Figure 10 (excitation wavelength) and on Figure 11 (fluorescence photons).

The positions, given by the angles between the illumination fiber and the detection fibers are: 180° (green), - 120° (blue) and + 120° (red).

The presence of the more absorbing volume on the measured TPSF at excitation wavelength is clearly seen on Figure 10, as suggested by the corresponding photon density map at 500 ps (Figure 9a).

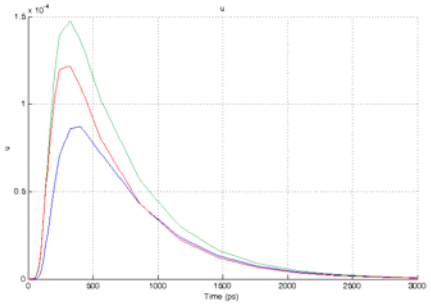

Figure 10. TPSF of excitation photons detected at 180° (green), - 120° (blue) and + 120° (red) from the illumination fiber.

It is a fact that, as regards cylindrical phantoms, the intensity and mean time of the fluorescence TPSF strongly depends on the position of the fluorochromes within the phantom, as shown on Figure 11.

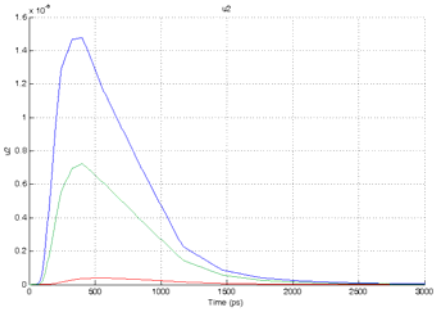

Figure 11. TPSF of fluorescence photons detected at 180° (green), - 120° (blue) and + 120° (red) from the illumination fiber.

These results demonstrate that the time profile detection and tomographic acquisitions used in our experimental setup allowed us to record data that are very sensitive to the distribution of fluorescent probes in an animal phantom, which is a prerequisite for the production of good-quality 3D preclinical images.

6. Conclusion

Comsol Multiphysics allows the computation of temporal profiles of excitation and fluorescence photons diffused in highly scattering media such as a living animal or a human organ. This program, generates m files, intended to be called by an optimization process, written in Matlab, to reconstruct images of the phantoms and animals to be investigated with our time-resolved tomography set up.

During the reconstruction process, the parameters of interest, (absorption and reduced scattering coefficients, fluorescent probe concentration) will be iteratively adjusted to perform constrained nonlinear minimization of an objective function of the distance between measured and computed temporal profiles. Applications are expected to concern preclinical imaging of brain diseases and cancer therapy models. Medical applications in neurology, cancer research and sport medicine are also considered.

7. References

1. T. Vo-Dinh, *Biomedical photonics handbook*, CRC Press, Boca Raton (2003).
2. A.P. Gibson, J.C. Hebden, S.R. Arridge, Recent advances in diffuse optical imaging, *Physics in Medicine and Biology*, **50**, R1-R43 (2005)
3. V. Ntziachristos, E.A. Schellenberger, J. Ripoll, D. Yessayan, E. Graves, A. Bogdanov, L. Josephson, R. Weissleder, Visualization of antitumor treatment by means of fluorescence molecular tomography with an annexin V-Cy5.5 conjugate, *Proceedings of the National Academy of Sciences*, **101**, 12294-12299 (2004)
4. S.L. Jacques, B.W. Pogue, Tutorial on diffuse light transport, *Journal of Biomedical Optics,* **13**, 041302 (2008)
5. B. Montcel, R. Chabrier, P. Poulet, A time resolved and multi-wavelength, fluorescence and diffuse optical tomography system for small animals, *Proceedings of SPIE*, **5859**, 132-140 (2005)
6. S.R. Arridge, Optical tomography in medical imaging, *Inverse Problems*, **15**, R41-R93 (1999)

8. Acknowledgements

The authors wish to thank Ms Nathalie Heider for thoroughly reading the manuscript.